ISSN: 2458-8989

Natural and Engineering Sciences

NESciences, 2025, 10 (1): 69-88 doi: 10.28978/nesciences.1631074

Synthesis of Phosphonated Solid Acid Catalyst from Water Hyacinth-Derived Carbon Dots and Its Catalytic Performance in 5-Hydroxymethylfurfural Production

Nardos Tesfalem Olango [1], Ballekallu Chinna Eranna [2], Belete Yilma Hirpaye [3*]

[1] Nardos Tesfalem Olango-College of Natural and Computational Sciences-Arbaminch University, Arbaminch, Ethiopia. E-mail: nardishatesfu@gmail.com

[2] Ballekallu Chinna Eranna-College of Natural and Computational Sciences-Arbaminch University, Arbaminch, Ethiopia. E-mail: ballekallu.china@amu.edu.et

[3*] Belete Yilma Hirpaye-College of Natural and Computational Sciences-Arbaminch University, Arbaminch, Ethiopia E-mail: belete.yilma@amu.edu.et

Abstract

The most effective parameters for the synthesis of Carbon Dots (CDs) obtained from Water Hyacinth (WH) were found to be 125℃, 35 minutes, and 7 g, with a maximum yield of 18.65%, according to the Design Expert 13.0 program. The phosphonated solid acid catalyst (PCDs) was synthesized by functionalizing CDs with concentrated phosphoric acid (85%) at 150℃ for 6 hours and used as a catalyst for producing 5–hydroxymethylfurfural (5-HMF). UV, XRD, SEM, FTIR, TGA elemental analysis, and acid–base titration techniques were used to characterize the CDs and catalyst. The FTIR spectra confirm the synthesized catalyst exhibited functional groups such as -PO3H2, -COOH, and -OH. The Catalytic Performance of PCDs was evaluated in the one-step Microwave-Assisted (MW) conversion of WH into 5-HMF using a biphasic solvent (isopropanol: water), achieving a 73.05% yield at 90℃ in 40 minutes using 0.6 g of catalyst. For using crude biomass in 5-HMF production this method offers a green and efficient approach.

Keywords:

Water hyacinth, carbon dots, solid acid catalyst, 5-HMF.

Article history:

Received: 19/10/2024, Revised: 19/12/2024, Accepted: 08/01/2025, Available online: 31/03/2025

*[3]*Corresponding Author: Belete Yilma Hirpaye, E-mail*: *belete.yilma@amu.edu.et*

Introduction

According to (Bhatia et al., 2021), the primary global energy sources are oil, natural gas and coal. However, the continued use of fossil fuels has resulted in environmental deterioration and an increasing energy deficit. Therefore, the development of safe, economical, environmentally friendly, and sustainable energy sources requires immediate attention. Renewable biomass (Saha & Abu-Omar, 2014)., particularly non-feed cellulosic biomass, shows potential as a sustainable option for producing liquid fuels and catalysts (Agar et al., 2020). Lignocellulosic biomass, which consists primarily of cellulose, hemicellulose, and lignin, is the most abundant renewable resource. Cellulose, the most prevalent natural carbohydrate polymer, makes up around 50 to 60% of its composition and β-1, 4-glycosidic linkages join the D-glucose units in this linear macromolecule (He et al., 2021; Ozyilmaz, 2023). Converting its derivatives into various biofuels and bio-based chemicals is anticipated to help alleviate energy shortages (Tiong et al., 2020; Deka et al., 2019).

The conversion of biomass, which is a bio-degradable, abundant, and cost-effective renewable resource into a heterogeneous catalyst to produce 5-Hydoxymethylfurfural (5-HMF) has great significance in decreasing high dependence on fossil fuel, reduce environmental pollution, improve economic stability (saving foreign currency), and provide job opportunity for societies (Tripathi *et al*., 2016). Water hyacinth (WH), bagasse, bamboo, and corncobs are among the most extensively studied sources of cellulose and hemicelluloses, with WH garnering particular attention (Carlini *et al.*, 2018; Nandini, 2024). WH biomass has been utilized in various applications, including biogas, briquettes, and bioethanol production. WH contains 19% hemicellulose, 55% cellulose, pectin, 14% lignin and 12% fat, oil, wax (Ewnetu Sahlie *et al.*, 2022).

5-HMF is widely regarded as a crucial intermediate compound derived from biomass and can be used in the production of various chemicals, including plastics, pharmaceuticals, fine chemicals, and liquid fuels (Fan *et al*., 2018). From 5-HMF, one can obtain several bio-derived compounds, like levulinic acid (LVA), 2,5-furan-dicarboxylic acid, 2,5-dimethylfuran, and 2,5-bis(hydroxymethyl)furan. A catalytic hydrogenolysis reaction converts 5-HMF to 2,5-dimethylfuran (2,5-DMF), the most attractive candidate for a biofuel, among 5-HMF's several applications (Khatiriet al., 2019). The previous study was conducted by (Bohre et al., 2015). The catalytic hydrolysis-dehydration of lignocellulosic biomass is primarily hindered by the catalyst's performance. While homogeneous catalysts like HCl, H_3PO_4, and H_2SO_4 have been utilized in the hydrolysis of lignocellulosic biomass, they encounter problems like, product separation, reactor corrosion, and waste effluent treatment. On the other hand, heterogeneous catalysts offer benefits such as simple product separation, efficient catalyst reusability, cost-effectiveness, environmentally friendly characteristics, and easy preparation methods. Although there has been notable advancement in producing by converting glucose and fructose into 5-HMF The three-step process of directly converting cellulose to 5-HMF has become increasingly difficult in recent years. Decomposing the cellulose into glucose is the initial stage. Converting glucose to fructose is the second step. The third step is to dehydrate the fructose. It is thought that Brønsted acid catalysis takes place in the first two steps, and a Lewis acid is used to catalyze the second step (Zhang et al., 2015). Converting cellulose into 5-HMF requires a highly active and selective catalytic system, which must be developed

immediately (In this work, the synthesized phosphonated solid acid catalyst (PCDs) bearing -PO_3H_2, -COOH, and phenolic -OH groups was generated by microwave-assisted (MW) carbonization of WH to synthesis CDs followed by phosphonation with concentrated H_3PO_4 acid (85 %) (Zümrütdal et al., 2022). PCDs facilitate the process of cellulose hydrolysis leading to glucose, fructose isomerization from glucose, and 5-HMF dehydration. They contain both Lewis acid sites and Brnsted acid sites (-PO3H2). With a low catalyst activity, this heterogeneous catalyst (PCDs) assists in the one-step MW-assisted synthesis of 5-HMF from cellulosic WH in a biphasic solvent system consisting of isopropanol and water (Mollazade, 2017; Majdanishabestari & Soleimani, 2019). This study could offer a promising approach for the extensive use of raw lignocellulosic biomass.

Materials and Methods

Materials

WH sample was taken from Abaya Lake located in Arba Minch town, Gamo Zone of Southern Ethiopia that was washed and dried at 80°C in oven for 24 hours till a standard weight was achieved. Then, the sample was ground into a fine powder using a miller and sieved through a 500-micrometer sieve to obtain the desired particle size. Concentrated phosphoric acid (85%,), 0.01M hydrochloric acid, 2M sodium chloride (99.9%, Riedelde Haen, Germany), 0.05M sodium hydroxide, Phenolphthalein, and Isopropanol. Throughout the experimental studies, chemicals and reagents were employed without further purification.

Experimental design for synthesis of carbon dots

A Box-Behnken design (BBD) with 3 variables, 3 levels, and 17 runs was used to find the optimal synthesis conditions for achieving the highest yield of CDs from WH powder (Table 1). Design Expert 13.0 software and Response Surface Methodology (RSM) were employed for data analysis, with carbonization temperature (A), carbonization time (B), and weight of WH powder (C) as the independent variables, and the percentage yield of CDs as the response variable (Peng *et al.,* 2020). The total number of experiments (N) for BBD was determined by using the equation (1).

$$N = K^2 + K + C_p \qquad 1$$

Where C_P is the replicate number of the central point and K is the variable number

Table 1. Experimental design result of actual versus predicted CDs QY response data

Independent variables (factors)			Dependent variables (responses)		
Run	Factor A: Temperature (oc)	Factor B: Time (minutes)	Factor C: Weight (g)	Actual QY (%)	Predicted QY (%)
1	125	45	8.5	16.45	16.61
2	150	45	7	14.92	14.97
3	125	45	8.5	16.67	16.61
4	100	45	7	8.52	8.60
5	100	45	10	6.40	6.35
6	100	60	8.5	7.45	7.34
7	125	60	10	12.98	13.14
8	125	45	8.5	16.65	16.61

9	100	30	8.5	4.59	4.67
10	125	45	8.5	16.69	16.61
11	150	60	8.5	15.08	15.00
12	150	45	10	13.76	13.68
13	125	60	7	18.65	18.68
14	125	30	10	13.45	13.42
15	150	30	8.5	10.59	10.70
16	125	45	8.5	16.59	16.61
17	125	30	7	11.60	11.44

Synthesis of CDs

The WH-derived carbon dots (CDs) were prepared using microwave-assisted treatment by mixing varying amounts of WH powder with distilled water and subjecting the mixture to carbonization with microwave energy at 100 watts for different time intervals and temperatures (Table 1). After carbonization, the material was filtered and centrifuged to separate the residue (Mies et al., 2007), and the resulting CDs powder was obtained (Briscoe et al., 2015) through oven-drying of the solution.

Determination of Carbon Dots Yield

The yield of CDs evaluated using equation 2.2.

$$Y_{CDs}\ (\%) = \frac{C}{Wp} \text{ x } 100 \qquad 2$$

Where: YCDs is the CDs yield in percent (%), C is the amount of synthesized CDs (g) at different variables, and WP is the initial weight of WH powder.

Synthesis of Catalyst (PCDs)

The catalyst synthesis was based on the method by Jori and Jadhav (2022), with modifications including the phosphonation of CDs using concentrated H3PO4 at temperatures between 110-190°C for 2-10 hours. The resulting solid was processed and labeled according to the phosphonation temperature and duration, with surface acid density identified as a key factor for determining high-performing catalysts.

Characterization of CDs and PCDs

The study followed ASTM D5373-02 (2003) to evaluate the composition of the WH in parts per million, analyzing moisture, ash, fixed carbon, and volatile matter using the Dumas method. The elemental composition was assessed, determining percentages of carbon, nitrogen, oxygen, hydrogen, and phosphorus. The catalyst preparation involved stirring NaCl with NaOH and monitoring the titer with Phenolphthalein. Functional groups in the CDs and catalyst were identified using FTIR spectroscopy, while XRD patterns were obtained with a Supernova single crystal X-ray diffractometer (Salame et al., 2018).. The morphology was analyzed with a scanning electron microscope (SEM), and thermal stability was assessed using thermogravimetric analysis at temperatures from 25 to 800°C. Additionally, UV-vis spectroscopy was employed to measure the concentration of 5-HMF and confirm the formation of CDs.

Evolution of Catalyst Performance in 5-HMF Production

The conversion of WH into 5-HMF was used as a benchmark to assess the catalytic activity of the phosphonated solid acid catalyst. Generally, 4 g WH powder and 0.5 g of the synthesized PCDs catalyst were combined adding 150 mL isopropanol-water biphasic solvent at ratios of 4:1. The mixture was subjected to a defined temperature and reaction period in the microwave. After, the 5-HMF was extracted from the organic phase using a rotary

evaporator and the remaining distillate was placed into a conical flask. The concentration of a resulted solution of 5-HMF was determined using UV-vis spectroscopy (Yi et al., 2014).

Quantification of 5-HMF Yield

The concentration of 5-HMF was determined using UV-vis spectroscopy at 284 nm wavelength with the standard curve method following the method reported by De Andrade et al. (2017). Standard solutions with known concentrations of 0.5, 0.7, 0.9, 1.1, 1.3, 1.5, and 1.7 mmol/L of 5-HMF were prepared and their absorbance was measured at 284 nm. The resulting linear curve was used to determine the concentration of 5-HMF in unknown samples. At least three replications of each finding were conducted, and average values were chosen. Based on a cellulose content of 55% in the WH (Ewnetu Sahlie et al., 2022), the yield of 5-HMF was determined as:

$$\text{5-HMF yield (\%)} = \frac{\text{5-HMF concentration in product}}{\text{Cellulose concentration in the loaded sample}} \text{ x } 100\%$$

Experimental Design and Statistical Analysis for 5-HMF Production

Using a BBD with RSM in Design Expert software version 13.0, optimal parameters for 5-HMF production were determined. The experimental design involved 17 runs with 5 replications at core locations. Independent variables (temperature, time, catalyst amount) were adjusted based on levels in Table 5. The response variable of 5-HMF yield percentage was used to assess combined effects. A regression model was used to create a 3D graphic, optimizing and clarifying factors impacting 5-HMF yield (Plengsaengsri et al., 2019).

Results and Discussions

Quantum Yields of Carbon Dots

The BBD method was used to conduct 17 experimental runs to synthesize CDs from WH. The actual and predicted results are shown in Table 1, with CDs yield ranging from 4.59% to 18.65%. These results align with a previous study reported by Bandi et al. (2016). Statistical analysis revealed significant differences in the QY responses of the experimental runs (p-value for QY: 0.000). Run 13 (A: 125 0c, B: 60 minutes, C: 7 g) yielded the highest CDs percentage (18.65%), while run 9 (A: 100 0c, B: 30 minutes, C: 8.5 g) yielded the lowest (4.59%). Table 1 demonstrates close agreement between actual and predicted values, indicating high compatibility.

Model Fitting and Statistical Analysis

Optimizing synthesis process, the BBD determined how carbonization time, WH weight and carbonization temperature affected CDs production. The yield figures, both actual and expected, from various process settings are displayed in Table 1. The model composed of second-order quadratic polynomials was generated using the Design Expert 13 program:

$$Y = \beta 0 + \sum \beta i\, Xi + \sum \beta ii Xi^2 + \sum \beta ij Xi Xj \qquad (3)$$

Here, linear slope is βi, βii reflects the quadratic effect for both variable Xi. β0 is constant coefficient, the interaction between Xi and Xj represented by βij. ε is a random error (Aslan and Cebeci, 2007). Based on the outcomes, the response, QY of CDs, can be represented as a quadratic regression model of weight of WH (C), carbonization temperature (A), carbonization time and (B):

$$QY\ (\%) = 16.61 + 3.42A + 1.74B - 0.8875C + 0.4075AB + 0.2400AC - 1.88BC - 5.23A^2 - 1.96B^2 - 0.4838C^2 \qquad (4)$$

The validity of the quadratic polynomial model was assessed using analysis of variance (Table 2). There was a highly significant model with only a 0.01% probability of happening owing to noise, as evidenced by the low P-value (< 0.0001) and high F-value (142.43). The determination coefficient (R2) was 0.9995, and the adjusted coefficient (adj-R2) of 0.9988 indicated a well-fitted model. The predicted coefficient (pre-R2) of 0.9933 also showed reasonable agreement. The coefficient of variation (CV) was low (1.13%), suggesting high reproducibility. The high p-value (0.1071) of lack of fit and adequate precision value of 124.7 indicated a reliable model. All linear, interaction and quadratic terms significantly affected the quantum yield (QY) (Table 4.2). Temperature, time, and weight of WH were the most significant variables affecting the QY of CDs. The quadratic model accurately described the linear relationship between synthesis conditions and QY (Figure 1a). The residual plot (Figure 1b) demonstrated satisfactory residuals, indicating a well-fitted model suitable for predicting QY.

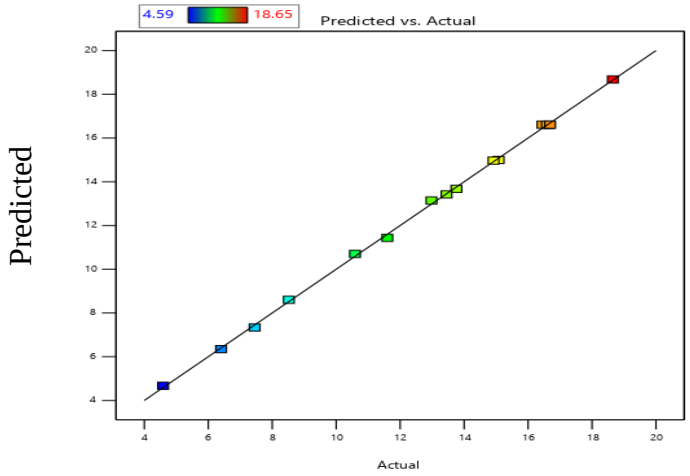

A

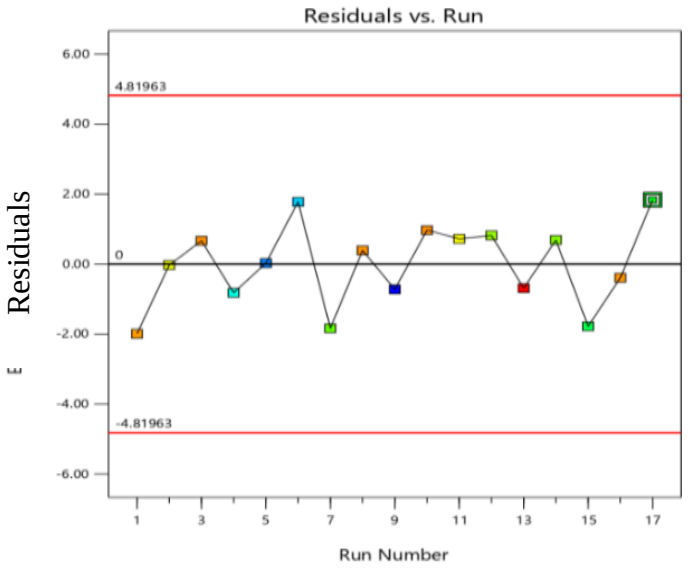

B

Figure 1. Diagnostic plot for developed model adequacy showing: a) actual versus predicted response for QY of CDs and b) residuals versus run number

Table 2. ANOVA results for response surface quadratic model

Source	Mean Square	Sum of Squares	F-value	Df	p-value	
Model	30.97	278.69	142.43	9	< 0.0001	significant
A	93.78	93.78	4368.23	1	< 0.0001	
B	24.26	24.26	1129.86	1	< 0.0001	
C	6.30	6.30	293.52	1	< 0.0001	
AB	0.6642	0.6642	30.94	1	0.0008	
AC	0.2304	0.2304	10.73	1	0.0136	
BC	14.14	14.14	658.55	1	< 0.0001	
A^2	115.01	115.01	5357.08	1	< 0.0001	
B^2	16.11	16.11	750.58	1	< 0.0001	
C^2	0.9853	0.9853	45.90	1	0.0003	
Residual	0.0215	0.1503		7		
Lack of Fit	0.0376	0.1127	4.00	3	0.1071	not significant
Pure Error	0.0094	0.0376		4		
Total		278.84		16		

Fit Statistics

Std. Dev.	0.1465	R^2	0.9995
Mean	38.00	Adjusted R^2	0.9988
C.V. %	0.3856	Predicted R^2	0.9933
		Adeq Precision	124.6607

Influence of Interactive Parameters on the CDs yields

- ***Influence of Temperature and Time***

The QYs of CDs were plotted as a 3D response surface, with carbonization temperature and time as variables. In Figure 2a, the QYs obtained with a constant weight of WH (8.5 g) were shown. Table 2 revealed a significant interaction between carbonization temperature and time, as indicated by a low p-value of 0.0008. The QY of CDs increased from 4.59% to 18.65% when the temperature was raised from 100 to 125 °C. The reason behind this is that QY increases as a result of complete carbonization, which is facilitated by greater temperatures (de Medeiros et al., 2019). The QY of CDs drops from 18.65% to 10.58% as the temperature rises higher. Yet, when the carbonization time was prolonged from 30 to 60 minutes, the QY of CDs rose dramatically, going from 4.59% to 18.65%. This implies that to get greater QYs, longer reaction times are required. The results show that raising the temperature promotes a more effective synthesis of QY when the reaction time is adequate (de Medeiros et al., 2019).

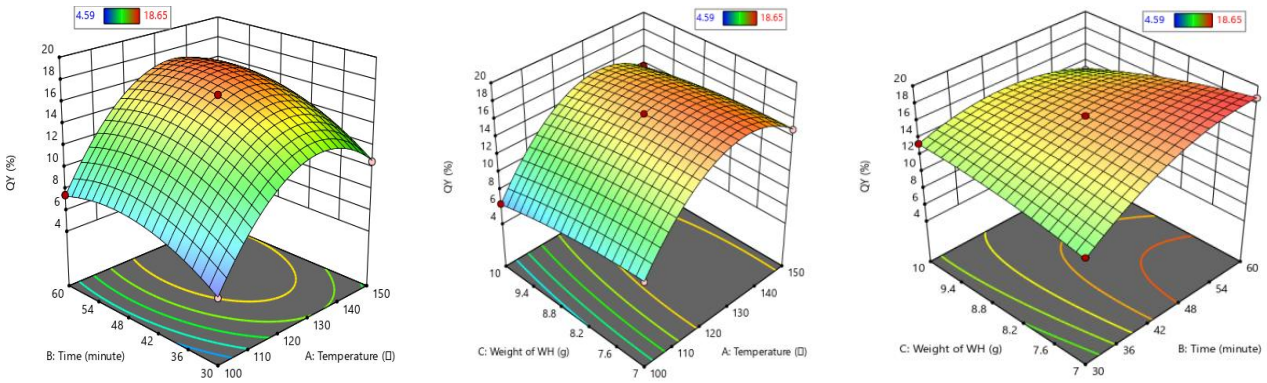

(a) (b) (c)

Figure 2: 3D Response surface plot (a) for the effect of temperature and time (b) effect of temperature and weight of WH and effect of temperature and weight of WH on QY of CDs.

- ***Influence of Temperature and Weight of WH***

A 3D response surface plot was utilized to illustrate the relationship between two variables while keeping one constant. At a constant carbonization time of 45 minutes, a surface plot was produced Figure 2b. Increasing the temperature up to 125 °C increased the percentage QY of CDs up to 18.65%, after which it fell, according to the data. The organic components in the starting material, WH, broke down at higher temperatures, which may have caused thermal deterioration and reduced the QY of the CDs, leading to this drop. The maximum QY of 18.65% was achieved at 125 °C. Furthermore, the highest QY of 18.65% was obtained when using a lower weight of WH (7 g), likely due to the enhanced solubility of WH at lower weights, ensuring maximum material availability for the CDs synthesis process (Ma et al., 2017).

- ***Influence of Time and Weight of WH***

The 3D response surface plot (Figure 2c) depicts the relationship between carbonization time and the weight of WH at a constant temperature of 1250c. A carbonization time of 60 minutes resulted in a maximum QY of CDs at 18.65%. The yield of CDs increased with a longer carbonization period, as greater time provided more opportunities for carbonization. In this study, a higher amount of CDs (18.65%) was synthesized within 60 minutes, attributed to the use of MW heating for CDs synthesis. The data indicates that an increase in time leads to a linear increase in QY. WH, being highly fibrous and cellulose-rich, a complex polysaccharide composed of glucose units. During extended carbonization, cellulose breaks down into simpler compounds such as L-glucose. The yield of CDs increases with longer carbonization times due to the availability of more reaction opportunities (Reza et al., 2014).

Optimization and Validation of Results

The experimental design aimed to find the best MW synthesis conditions for achieving the highest QY through the carbonization of WH. Design-Expert 13.0 software was used for numerical optimization, resulting in the best condition of 131.73 °C, 53.17 minutes, and 7.20 g of WH (Figure 3a). At these conditions, the predicted QY was 18.82%. Three experiments conducted at these conditions produced an average QY of 18.77%, closely matching the predicted maximum QY of 18.81%. This validates the model's accuracy in explaining the relationship between operating factors and the response (Issa et al., 2020).

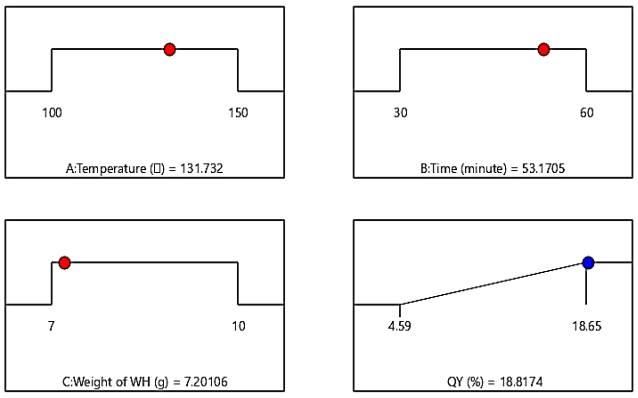

(a)

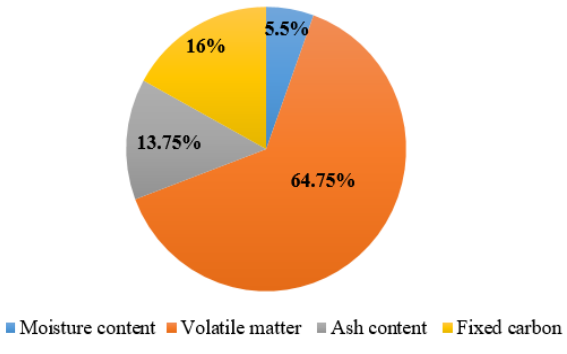

(b)

Figure 3. Ramp desirability plot optimization of the variables for the best of CDs yield

Characterization of CDs and Catalyst

Figure 3b displays the proximate analysis results, which were consistent with findings in (Huang et al.,2018). A low moisture content is recommended for catalytic conversion processes, as high moisture content can hinder catalytic activity by interacting with the water molecule instead of the catalyst. In this study, the moisture content of WH is 5.5%.

The high volatile matter content of WH (64.75%) indicates its reactivity during the carbonization process, making it susceptible to burning. Conversely, a low volatile matter value suggests that biomass is hard to burn or affects its reactivity.

The low ash content of WH (13.75%) is beneficial for reducing sludge formation during the synthesis of 5-HMF. The ratio of volatile matter to fixed carbon is a crucial parameter for assessing biomass reactivity. Biomass commonly has a ratio of VM/FC > 4.0 (Gil et al., 2010). In this study, the ratio of volatile matter to fixed carbon for WH biomass is 4.5, indicating its high reactivity.

The maximum surface acid density of the PCDs catalyst was recorded as 1.415 mmol/g (Table 3). The elemental composition of CDs and solid acid catalyst can be accurately determined through ultimate analysis, with a phosphorus content of 2.43 % as shown in Table 4. The carbon concentration of the CDs catalyst is higher than that of the PCDs catalyst. After phosphonation, the oxygen and phosphorus contents notably increase, indicating the grafting of phosphonic acid groups on the surface of CDs, leading to more active sites, higher surface acid density, and enhanced catalytic activity (Of et al., 2017). UV–vis absorption spectra (Figure 4a), showed a notable peak at about 288 nm which is associated with the n-π* transition of OH and carboxylic acid (COOH) groups found on the CDs' surfaces. A number of oxygenated functional groups are thus passivated onto the surface of the CDs (Prathumsuwan et al., 2019). According to (Park et al. 2014), the FTIR spectra of CDs (Figure 4b) displayed a distinctive peak at 3407 cm-1, which is thought to be caused by the O-H stretching bands. According to (Zhu et al., 2012), the stretching vibrations of C=O were the cause of the peak at 1625 cm−1. In addition, the presence of carboxylic functional groups was further supported by the signal at 1066 cm−1, which suggested C-O stretching. The peak at 1409 cm−1 and the shoulders at 2934 cm−1 were identified as the stretching vibrations of C=C and C-H, respectively. When the PCDs catalyst was phosphonated, the FTIR spectra shown in Figure 4b showed the presence of C-P, P-O, and P=O bands at 1450, 1195, and 1074 cm−1, respectively. Raghu et al. (2019) confirmed that phosphonic groups were incorporated onto the surface of CDs following phosphonation, as the signal at 1074 cm−1 suggested the symmetric P=O stretching vibration. A broad diffraction peak at 2θ = 15-30 Ɗ was observed in the XRD patterns of the CDs and catalyst (Figure 4c), which is typically associated with amorphous carbon. This type of carbon is made up of aromatic carbon sheets that are arbitrarily organized, as stated by (Fu et al., 2012). The surface morphology of the CDs and catalyst was investigated using the SEM technique (Figure 5a, b). The SEM images of the CDs depicted an irregular compact structure with particles resembling grains covered in a thick foreign embodiment, showing minimal visible porous structures and relatively high surface areas (Figure 5a). Upon H3PO4 functionalization, the PCDs catalyst exhibited a well-developed porous surface structure and smaller surface area, which can be attributed to the dehydration effect of H3PO4 and the oxidation of organic compounds in the phosphonation step (Figure 5b). Additionally, SEM images for the PCDs catalyst indicated that the white parts of the surface represented the inorganic composition (Jamil et al., 2020). Additionally, it was observed that the CDs had a particle size of less than 10 nm (Figure 5c). The solid acid catalysts' thermal stability was tested using TGA, as shown in Figure 5d. The desorption of physically adsorbed moisture in the catalyst, leading to a 1.5% weight loss in the temperature range from the start to 125℃ (event 1), is mostly caused by the hydrophilicity of the -PO3H2 groups linked to the carbon

surface, as shown by the TG curves (Rana et al., 2019). Afterward, a noticeable reduction in weight of the catalyst from 250 to 600 ℃ (event 2), is 60.13% and described how hemicellulose, cellulose, and partly lignin break down thermally to release chemical bonds. A curve showing the constant loss of weight from 610 to 800 °C (event 3) indicates the thermal breakdown of oxygenated functional groups (Jamil et al., 2020). This result confirms that under the hydrolysis-dehydration reaction, PCDs catalyst produced from WH shows satisfactory thermal stability, particularly below 100 ℃.

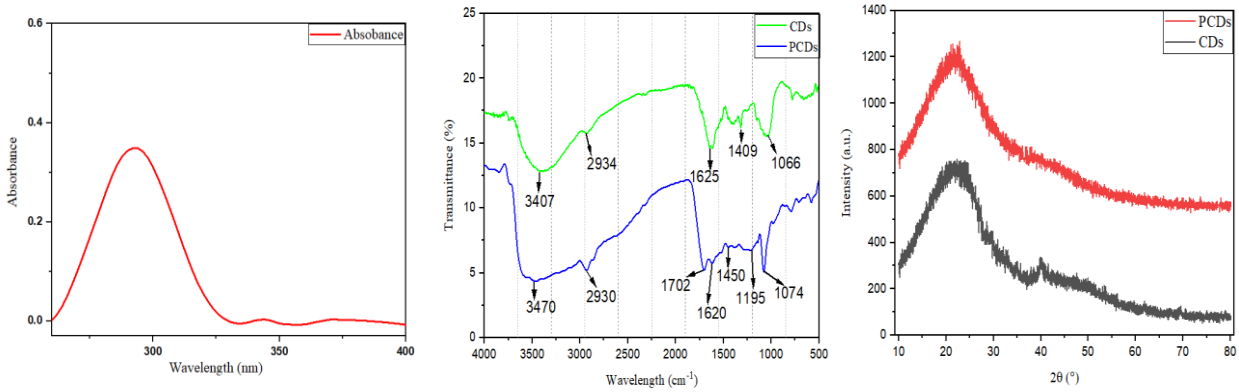

(a) (b) (c)

Figure 4. (a) UV-visible spectra of CDs (b) FTIR spectrum of CDs and PCDs (c) XRD pattern of CDs and PCDs

Table 3. Surface acid density (-PO3H2) group of the catalyst

Catalysts	Surface acidity (mmol/g)	Catalysts	Surface acidity (mmol/g)
PCDs(110)-(4)	1.245	PCDs(150)-(2)	1.283
PCDs(130)-(4)	1.298	PCDs(150)-(4)	1.382
PCDs(150)-(4)	1.382	PCDs(150)-(6)	1.415
PCDs(170)-(4)	1.332	PCDs(150)-(8)	1.381
PCDs(190)-(4)	1.299	PCDs(150)-(10)	1.362

Table 4. Ultimate analysis of CDs and PCDs catalyst

Samples	C (%)	H (%)	N (%)	P (%)	O (%)
CDs	50.04	4.25	1.34	0.03	44.34
PCDs (150)-(6)	40.89	2.44	0.84	2.43	53.4

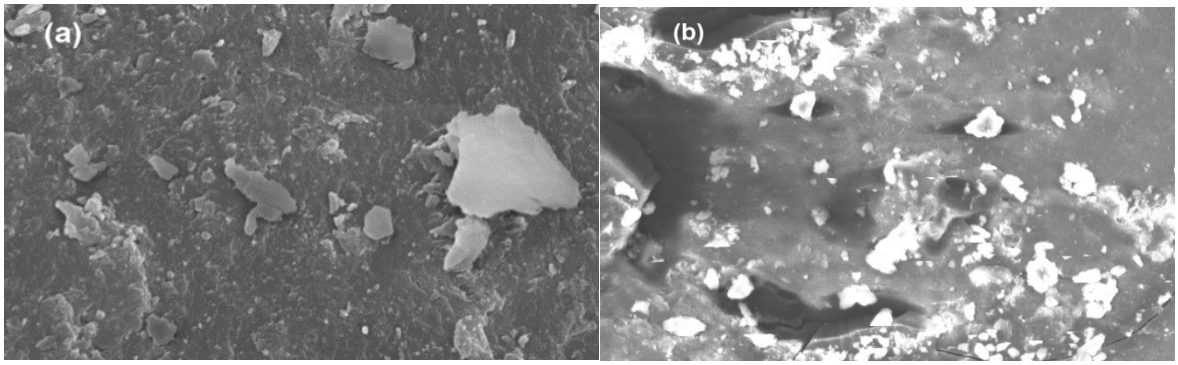

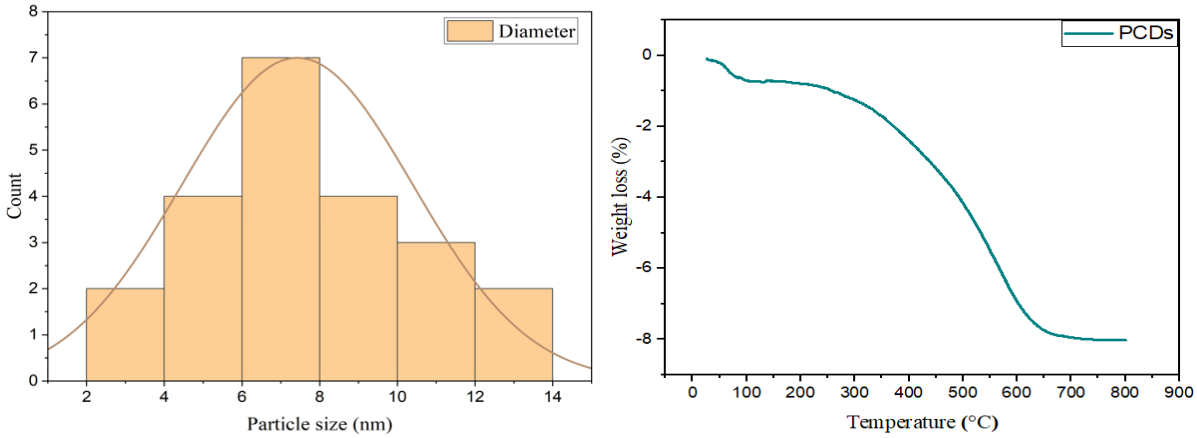

Figure 5: SEM images of (a) CDs (b) PCDs catalyst (c) size distributions of CDs and (d) TG curve of PCDs catalyst

Optimization of Phosphonation Parameters

- ***Effect of Phosphonation Temperature***

The effect of phosphonation temperature on surface acidity of the synthesized catalyst is quantified and results are reported in Figure 6a. As a response, the surface acid density values of the catalysts were evaluated. The surface acidity tests were performed at phosphonation duration of 4 hours. The quantity, position, and stability of the attachment of -PO3H2 groups within the CDs structure are all influenced by the phosphatation temperature. The introduction of -PO3H2 groups may be inhibited by extreme heat because it can cause side reactions and the collapse of the carbon skeleton (Yu et al., 2017). However, the phosphonated product resulted at lower temperatures is unstable and easily to be decomposed. As demonstrated in Figure 6a, from 110 °C to 150 °C, the surface acidity increases first, reaching a maximum value of 1.382 mmol/g at 150 °C. Afterwards, the surface acidity of the catalyst drops to 1.273 mmol/g when the phosphonation temperature is raised further. Consequently, 150 °C is determined to be the optimal phosphonation temperature.

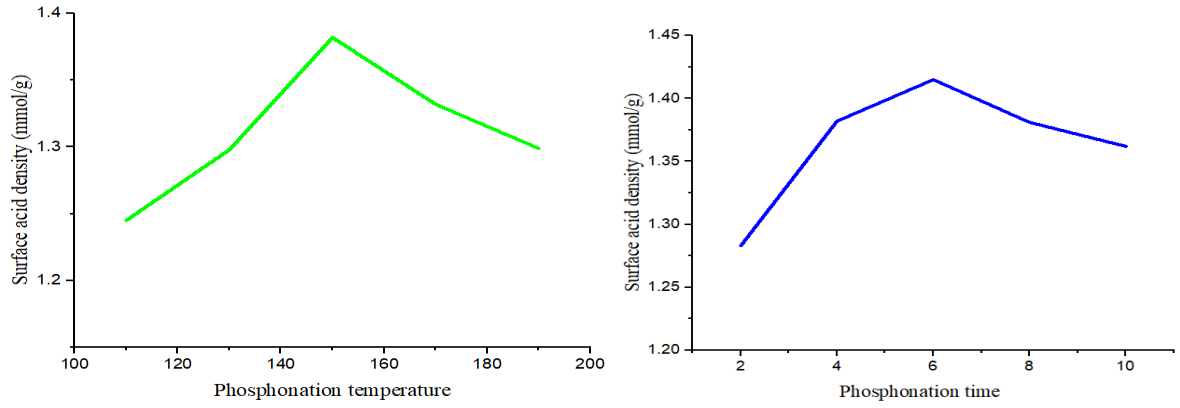

(a) (b)

Figure 6: (a) Effect of phosphonation temperature (phosphonation time, 4 hours) (b) Effect of phosphonation time (phosphonation temperature, 150 °C) on surface acid density of catalyst.

- ***Effect of Phosphonation Time***

The functionalization of the CDs is time-dependent, as seen in Figure 6b, and this is further clarified by looking at the surface acid density values of the catalysts. It is evident that the phosphonation is responsible for the presence of acid sites in the catalysts. At a phosphonation temperature of 150 °C, tests were performed to compare the effect of phosphonation time on surface acidity. Phosphonation times ranging from 6 to 10 hours show an increase in surface acid density values reaching 1.415 mmol/g, before gradually decreasing to 1.362 mmol/g. Da Luz Corrêa et al. (2020) found that after 6 hours of phosphonation, the functionalization process may have reached saturation. As a result, appropriate conditions for synthesis of phosphonated solid acid catalyst from WH-derived CDs were found to be a phosphonation temperature of 150 °C and a phosphonation time of 6 hours.

Evolution of Catalyst Performance in 5-HMF Production

Based on the optimal process conditions (phosphonation temperature: 150 °C and time: 6 hours), the best catalyst was chosen for suitable conversion of WH to 5-HMF. For the control experiment, 4 g WH was left to react in the MW reactor for 30 minutes at 70°C with 150 mL of isopropanol: water biphasic solvent, but no catalyst was added. The results showed that just 2% of the original material, 5-HMF, was formed. The remaining trials involved adding 4 grams of cellulosic WH to the reactor along with 0.5 grams of catalyst. The next step was to add 150 mL of isopropanol: water and boil the mixture at 70°C for 30 minutes. According to Dulie et al. (2021), the highest yield of 5-HMF in the biphasic solvent system was 34%. We ran each of the catalytic performance tests three times.

Spectral Characteristics of 5-HMF

UV light can be absorbed by 5-HMF, and its concentration can be accurately measured using UV spectroscopy as long as there is no spectral interference. The absorption of standard 5-HMF at 284 nm follows linear regression analysis well (Figure 7a), allowing for precise concentration measurements. Figure 7b shows that 5-HMF can be accurately measured by UV spectroscopy because of its significant absorption in the UV range below 330 nm, when its characteristic absorption happens at roughly 284 nm (Chi et al., 2009).

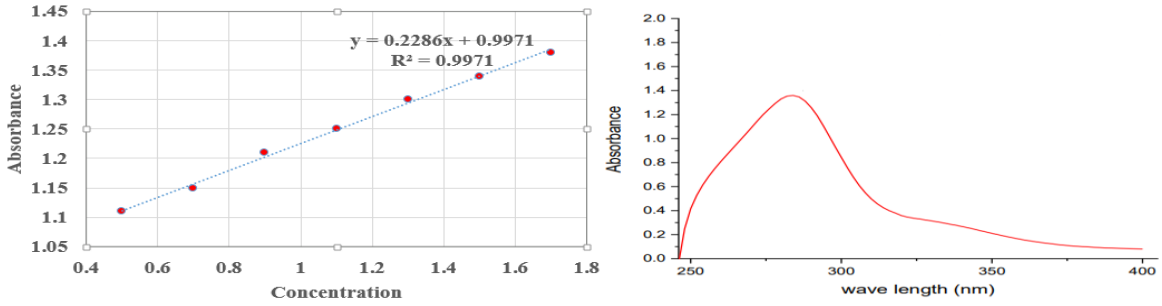

(a) (b)

Figure 7: (a) Standard curve for 5-HMF and (b) Spectra of the produced 5-HMF.

RSM Optimization of 5-HMF Production

The BBD response surface method optimized three production variables (temperature, time, and catalyst amount) for 5-HMF yield. Experimental results showed the lowest yield (34.01%) at run 2 and the highest yield (73.05%) at run 10, consistent with previous (Chareonlimkun et al., 2010). Table 5 compares predicted and

actual results, indicating a strong correlation. This demonstrates the efficiency of the synthesis process for 5-HMF from WH in the MW-biphasic solvent-solid acid catalyst system.

- ***Model Fitting and Statistical Analysis***

An ANOVA analysis was conducted to assess the reliability, reproducibility, and efficiency of the regression models developed in this study (Equation 3.3). Table 6 provides an overview of the ANOVA analysis results for the 5-HMF yield.

$$Y\ (\%) = 71.43 + 0.9288A + 3.04B + 8.19C + 1.08AB - 2.16\ AC + 7.50BC - 20.72\ A^2 - 12.94\ \ B^2 - 6.16C^2 \quad (5)$$

The quadratic model was evaluated using ANOVA, with results summarized in Table 6. The model represents the statistical significance of F-value 373.51. The F-value could high due to noise with 0.01%. significant model terms are represented by p-values which are less than 0.0500. Some important model terms are AC, BC, A^2, B^2, C^2 A, B, and C. If the values are more than 0.1000 the model term are not considered as significant. When compared to the pure error, the Lack of Fit F-value of 1.02 indicates that the Lack of Fit is not significant enough to justify consideration. An F-value for Lack of Fit this high could be the result of random chance, which occurs 47.27 percent of the time. A lack of fit that is not statistically significant is considered good. There is less than 0.2 between the Adjusted R^2 and the Predicted R^2, thus we can say that they are reasonably in agreement with each other. Adequate Precision measures the signal to noise ratio. In this study, the adequate precision value of 46.93 suggests the best fitness of the developed model. Diagnostic plots, such as Figure 8a and Figure 8b were used to assess the reliability of the quadratic model across the range of experiments. The model-predicted values in Figure 8a exhibit a strong correlation (R2 = 0.9979) with the experimental data, indicating that the model accurately estimates the experimental yield values.

Table 6. ANOVA results for response surface quadratic model

Source	Sum of Squares	Df	Mean Square	F-value	p-value	
Model	3779.60	9	419.96	373.51	< 0.0001	significant
B	73.99	1	73.99	65.81	< 0.0001	
C	536.94	1	536.94	477.55	< 0.0001	
A	6.90	1	6.90	6.14	0.0424	
AC	18.71	1	18.71	16.64	0.0047	
BC	225.15	1	225.15	200.25	< 0.0001	
AB	4.67	1	4.67	4.15	0.0811	
B^2	705.46	1	705.46	627.44	< 0.0001	
C^2	159.85	1	159.85	142.17	< 0.0001	
A^2	1808.35	1	1808.35	1608.34	< 0.0001	
Residual	7.87	7	1.12			
Lack of Fit	3.41	3	1.14	1.02	0.4727	not significant
Pure Error	4.46	4	1.12			
Total	3787.47	16				

Fit Statistics

Std. Dev.	1.06	R^2	0.9979
Mean	52.68	Predicted R^2	0.9838
C.V. %	2.01	Adjusted R^2	0.9953
		Adeq Precision	46.9338

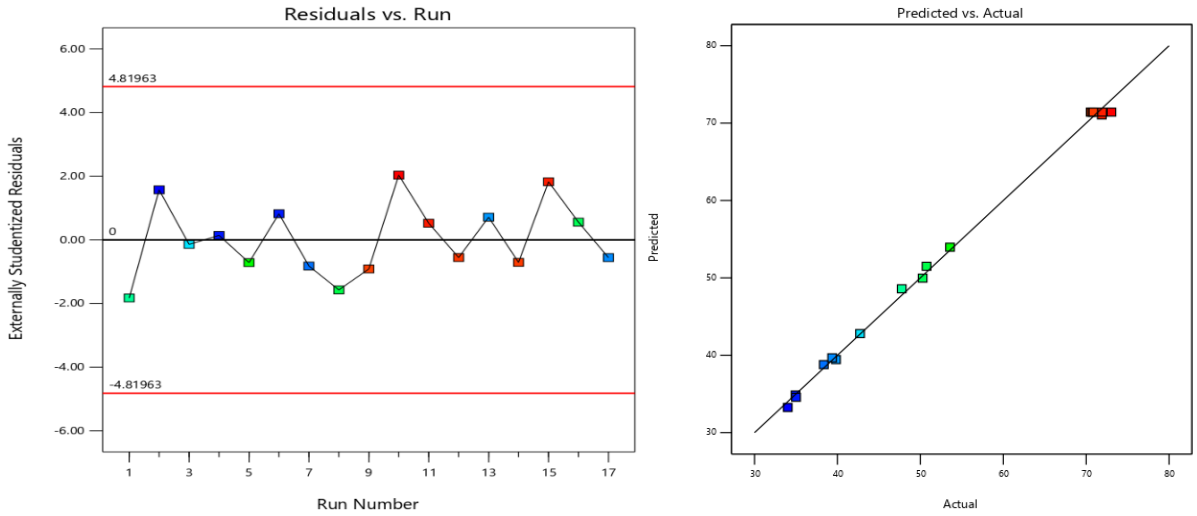

Figure 8. Diagnostic plots of (a) Predicted vs. actual yield of 5-HMF, (b) residuals versus run number

Influence of Interactive Parameters on the yield of 5-HMF

- ***Effect of Temperature and Time***

The impact of variables on 5-HMF yield is shown in Figure 9a by means of three-dimensional response surface plots. In order to find the interacting effects, we adjusted the other two variables within certain ranges while holding one variable constant. Experiments were optimized by using a catalyst amount of 0.6 g, a radiation time range of 20-60 minutes, and a reaction temperature range of 70-110°C. The yield of 5-HMF grew steadily until it reached a maximum as the temperature and time were raised, maintaining a constant catalyst quantity of 0.6 g. Results showed that at 90°C, 5-HMF had a very high yield (73.05%). However, the yield decreases with additional time and temperature rises, suggesting that 5-HMF may degrade or polymerize. High temperatures arise while it intermediates cross-polymerization and polymerization of 5-HMF, are likely the causes of the generation of by-products. According to (Li et al., 2020), this is the reason behind the lower 5-HMF yield observed in this investigation.

- ***Effect of Temperature and Amount of Catalyst***

Figure 9b depicts 3D response surface plots showing the combined impact of temperature and catalyst quantity on 5-HMF yield, with time held constant at 40 minutes. The plot illustrates that increasing the catalyst amount notably enhances the 5-HMF yield, rising from 34.95% to 73.05% as the catalyst amount increases from 0.5 to 0.6 (Table 5). However, very high temperatures and large catalyst amounts are unsuitable for 5-HMF production, as indicated in Figure 9b. Initially, higher temperature or catalyst amounts boost 5-HMF yield, but beyond a certain point, further increases reduce the yield. This could be attributed to side reactions competing with the desired glucose-to-5-HMF conversion, possibly caused by excessive acid-active sites promoting undesired by-products like humins, levulinic acid, or formic acid. (Shao et al., 2021).

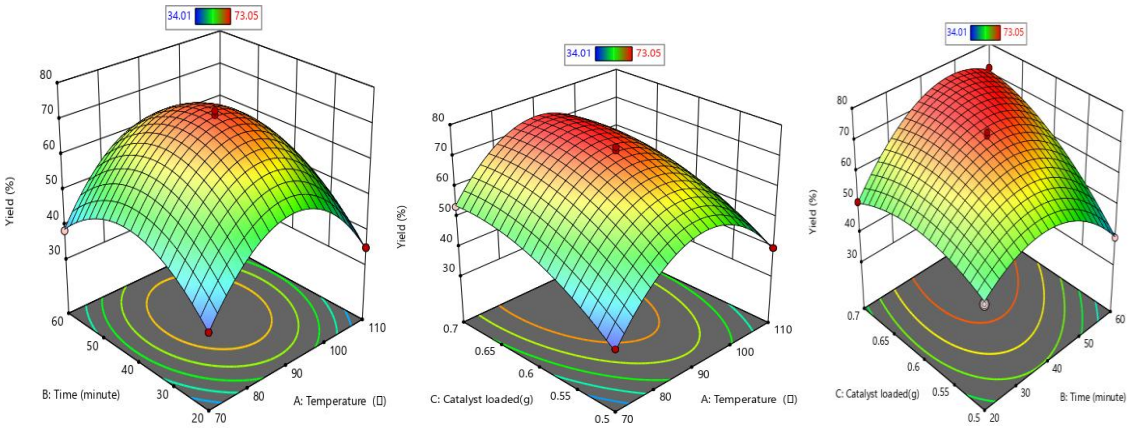

(a) (b) (c)

Figure 9. 3D Response surface plot (a) for the effect of temperature and time (b) effect of temperature and amount of catalyst, and the effect of time and amount of catalyst on the yield of 5-HMF

Table 5. Experimental design result of actual versus predicted 5-HMF yield response data

Independent variables (factors)			Dependent variables (responses)		
Runs	Factor A: Temperature (oC)	Factor B: Time (minutes)	Factor C: Amount of catalyst (g)	Actual yield (%)	Predicted yield (%)
1	90	20	0.5	47.76	48.59
2	70	40	0.5	34.01	33.26
3	110	60	0.6	42.73	42.81
4	70	20	0.6	34.95	34.87
5	70	40	0.7	53.58	53.97
6	110	20	0.6	35.01	34.57
7	70	60	0.6	38.35	38.79
8	110	40	0.7	50.75	51.50
9	90	40	0.6	70.55	71.42
10	90	40	0.6	73.05	71.42
11	90	40	0.6	71.94	71.42
12	90	40	0.6	70.87	71.42
13	110	40	0.5	39.83	39.44
14	90	40	0.6	70.73	71.42
15	90	60	0.7	71.89	71.06
16	90	20	0.7	50.28	49.97
17	90	60	0.5	39.36	39.67

- ***Effect of Time and Amount of Catalyst***

In Figure 9c, the 3D surface plot illustrates the impact of radiation time and amount of catalyst on 5-HMF yield at a constant temperature of 90 °C. The plot shows that increasing radiation time gradually enhances the 5-HMF yield, with a notable increase from 20 to 40 minutes. However, further increases in time lead to a decline in yield to 39.58%, likely due to prolonged reaction favoring the conversion of 5-HMF into other compounds. The RSM analysis confirms the highly essential interaction effect between radiation time and catalyst amount in determining 5-HMF yield ($p < 0.0001$) (Zhang et al., 2017).

Optimization and validation of process parameters

The numerical optimization method was employed to optimize the production process variables for 5-HMF yield. A catalyst amount of 0.637 g and temperature of 88.97 °C, a time of 41.66 minutes were obtained in optimal condition and, resulting in a predicted yield of 73.96% with a desirability of 1.000, as depicted in Figure 10. To validate the reliability of the optimized conditions and the software's ability to predict optimum responses, triplicate conducted experiments using selected optimal conditions. Across all trials, the average production of 5-HMF was 73.75%. According to Abdullah Issa et al. (2020), this validation result verifies that the model that was created using the BBD and RSM adequately describes the connection between the operational parameters and the response.

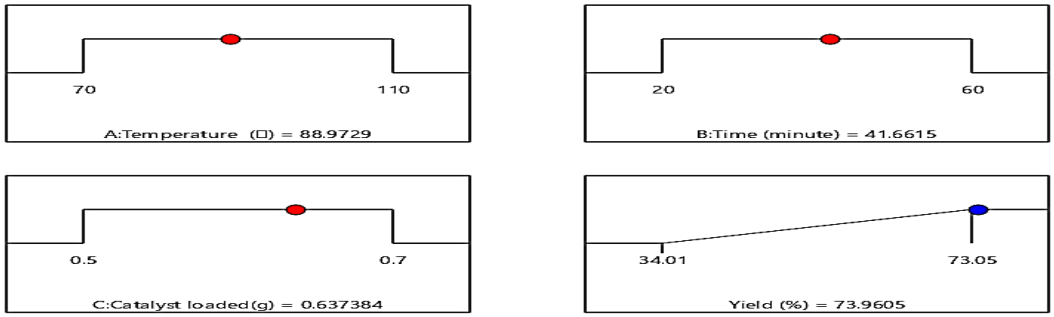

Figure 10. Ramp desirability plot optimization of the variables (temperature: (°C), time: (minutes), and catalyst loaded (g).

Conclusion

The best conditions for creating CDs were determined by running the synthesis at a temperature of 120°C for 60 minutes and using a regression model from the response surface desirability optimization technique. The weight of WH should be 7 g. CDs was efficiently synthesized from WH through MW-assisted carbonization, achieving a yield of up to 18.65 % under optimized conditions. The PCDs catalyst was synthesized by functionalizing CDs with concentrated H3PO4 (85%) under optimal conditions of 150 °C for 6 hours. The resulting solid acid catalyst, bearing -PO3H2, -OH, and -COOH functional groups, exhibited suitable Lewis and Brønsted acid sites, with smaller surface area and pore volume. This catalyst displayed high catalytic activity in the one-step MW-assisted 5-HMF production from WH in an isopropanol: water biphasic reaction medium. It also demonstrated thermal stability below 100°C and a high surface acid density of 1.415 mmol/g. XRD analysis revealed that the catalyst exhibited amorphous characteristics with low graphitization, which is favorable for catalytic activity in the hydrolysis-dehydration reaction. The catalyst showed promising performance in the production of 5-HMF from WH, with a yield reaching up to 73.05% under the optimized conditions, indicating its potential for industrial-scale production processes.

References

Agar, D. A., Svanberg, M., Lindh, I., & Athanassiadis, D. (2020). Surplus forest biomass–The cost of utilisation through optimised logistics and fuel upgrading in northern Sweden. *Journal of cleaner production*, *275*, 123151. https://doi.org/10.1016/j.jclepro.2020.123151.

Aslan, N. E. V. Z. A. T., & Cebeci, Y. A. K. U. P. (2007). Application of Box–Behnken design and response surface methodology for modeling of some Turkish coals. *Fuel*, *86*(1-2), 90-97. https://doi.org/10.1016/j.fuel.2006.06.010

Bhatia, S. K., Palai, A. K., Kumar, A., Bhatia, R. K., Patel, A. K., Thakur, V. K., & Yang, Y. H. (2021). Trends in renewable energy production employing biomass-based biochar. *Bioresource Technology, 340.* https://doi.org/10.1016/j.biortech.2021.125644.

Bohre, A., Dutta, S., Saha, B., & Abu-Omar, M. M. (2015). Upgrading furfurals to drop-in biofuels: An overview. *ACS Sustainable Chemistry & Engineering*, *3*(7), 1263-1277.

Briscoe, J., Marinovic, A., Sevilla, M., Dunn, S., & Titirici, M. (2015). Biomass-derived carbon quantum dot sensitizers for solid-state nanostructured solar cells. *Angewandte Chemie International Edition*, *54*(15), 4463-4468. https://doi.org/10.1002/anie.201409290

Carlini, M., Castellucci, S., & Mennuni, A. (2018). Water hyacinth biomass: Chemical and thermal pre-treatment for energetic utilization in anaerobic digestion process. *Energy Procedia*, *148,* 431-438. https://doi.org/10.1016/j.egypro.2018.08.106

Chareonlimkun, A., Champreda, V., Shotipruk, A., & Laosiripojana, N. (2010). Catalytic conversion of sugarcane bagasse, rice husk and corncob in the presence of TiO2, ZrO2 and mixed-oxide TiO2–ZrO2 under hot compressed water (HCW) condition. *Bioresource technology*, *101*(11), 4179-4186. https://doi.org/10.1016/j.biortech.2010.01.037

Chi, C., Zhang, Z., Chang, H. M., & Jameel, H. (2009). Determination of furfural and hydroxymethylfurfural formed from biomass under acidic conditions. *Journal of Wood Chemistry and Technology*, *29*(4), 265-276. https://doi.org/10.1080/02773810903096025

da Luz Corrêa, A. P., Bastos, R. R. C., da Rocha Filho, G. N., Zamian, J. R., & da Conceição, L. R. V. (2020). Preparation of sulfonated carbon-based catalysts from murumuru kernel shell and their performance in the esterification reaction. *RSC advances*, *10*(34), 20245-20256. https://doi.org/10.1039/D0RA03217D

de Andrade, J. K., de Andrade, C. K., Komatsu, E., Perreault, H., Torres, Y. R., da Rosa, M. R., & Felsner, M. L. (2017). A validated fast difference spectrophotometric method for 5-hydroxymethyl-2-furfural (HMF) determination in corn syrups. *Food chemistry*, *228*, 197-203. https://doi.org/10.1016/j.foodchem.2017.01.158

de Medeiros, T. V., Manioudakis, J., Noun, F., Macairan, J. R., Victoria, F., & Naccache, R. (2019). Microwave-assisted synthesis of carbon dots and their applications. *Journal of Materials Chemistry C*, *7*(24), 7175-7195.

Deka, M. J., Dutta, P., Sarma, S., Medhi, O. K., Talukdar, N. C., & Chowdhury, D. (2019). Carbon dots derived from water hyacinth and their application as a sensor for pretilachlor. *Heliyon*, *5*(6). https://doi.org/10.1016/j.heliyon.2019.e01985

Dulie, N. W., Woldeyes, B., & Demsash, H. D. (2021). Synthesis of lignin-carbohydrate complex-based catalyst from Eragrostis tef straw and its catalytic performance in xylose dehydration to furfural. *International Journal of Biological Macromolecules*, *171,* 10-16. https://doi.org/10.1016/j.ijbiomac.2020.12.213

Ewnetu Sahlie, M., Zeleke, T. S., & Aklog Yihun, F. (2022). Water Hyacinth: A sustainable cellulose source for cellulose nanofiber production and application as recycled paper reinforcement. *Journal of Polymer Research*, *29*(6), 230. https://doi.org/10.1007/s10965-022-03089-0

Fan, G., Wang, Y., Hu, Z., Yan, J., Li, J., & Song, G. (2018). Synthesis of 5-hydroxymethyl furfural from cellulose via a two-step process in polar aprotic solvent. *Carbohydrate polymers*, *200*, 529-535. https://doi.org/10.1016/j.carbpol.2018.08.043

Fu, Z., Wan, H., Hu, X., Cui, Q., & Guan, G. (2012). Preparation and catalytic performance of a carbon-based solid acid catalyst with high specific surface area. *Reaction Kinetics, Mechanisms and Catalysis*, *107*(1), 203-213. https://doi.org/10.1007/s11144-012-0466-9

Gil Matellanes, M. V., Casal Banciella, M. D., Pevida García, C., Pis Martínez, J. J., & Rubiera González, F. (2010). Thermal behaviour and kinetics of coal/biomass blends during co-combustion. http://doi.org/10.1016/j.biortech.2010.02.008

He, Q., Lu, Y., Peng, Q., Chen, W., Fan, G., Chai, B., & Song, G. (2021). Synthesis of 5-hydroxymethylfurfural from fructose catalyzed by sulfonated carbon-based solid acid. *Biomass Conversion and Biorefinery*, 1-9. https://doi.org/10.1007/s13399-021-01847-6

Huang, L., Xie, C., Liu, J., Zhang, X., Chang, K., Kuo, J., ... & Evrendilek, F. (2018). Influence of catalysts on co-combustion of sewage sludge and water hyacinth blends as determined by TG-MS analysis. *Bioresource technology*, *247*, 217-225. https://doi.org/10.1016/j.biortech.2017.09.039

Issa, M. A., Abidin, Z. Z., Sobri, S., Abdul-Rashid, S., Mahdi, M. A., Ibrahim, N. A., & Pudza, M. Y. (2020). Fabrication, characterization and response surface method optimization for quantum efficiency of fluorescent nitrogen-doped carbon dots obtained from carboxymethylcellulose of oil palms empty fruit bunch. *Chinese Journal of Chemical Engineering*, *28*(2), 584-592. https://doi.org/10.1016/j.cjche.2019.04.003

Jamil, F., Ala'a, H., Naushad, M., Baawain, M., Al-Mamun, A., Saxena, S. K., & Viswanadham, N. (2020). Evaluation of synthesized green carbon catalyst from waste date pits for tertiary butylation of phenol. *Arabian journal of chemistry*, *13*(1), 298-307. https://doi.org/10.1016/j.arabjc.2017.04.009

Jori, P. K., & Jadhav, V. H. (2022). Highly Efficient Zirconium Based Carbonaceous Solid Acid Catalyst for Selective Synthesis of 5-HMF from Fructose and Glucose in Isopropanol as a Solvent. *Catalysis Letters*, *152*(6), 1703-1710. https://doi.org/10.1007/s10562-021-03764-9

Khatiri, K., Sheikh, A., Hesam, R., & Alikhani, N. (2019). The Role of Participation in Preventing the Water Crisis. *International Academic Journal of Innovative Research*, *6*(1), 47–52. https://doi.org/10.9756/IAJIR/V6I1/1910004

Li, M., Jiang, H., Zhang, L., Yu, X., Liu, H., Yagoub, A. E. A., & Zhou, C. (2020). Synthesis of 5-HMF from an ultrasound-ionic liquid pretreated sugarcane bagasse by using a microwave-solid acid/ionic liquid system. *Industrial Crops and Products*, *149*, 112361. https://doi.org/10.1016/j.indcrop.2020.112361.

Ma, X., Dong, Y., Sun, H., & Chen, N. (2017). Highly fluorescent carbon dots from peanut shells as potential probes for copper ion: The optimization and analysis of the synthetic process. *Materials Today Chemistry*, *5*, 1-10. https://doi.org/10.1016/j.mtchem.2017.04.004

Majdanishabestari, K., & Soleimani, M. (2019). Using simulation-optimization model in water resource management with consideration of environmental issues. *International Academic Journal of Science and Engineering*, *6*(1), 15–25. https://doi.org/10.9756/IAJSE/V6I1/1910002

Meng, W., Bai, X., Wang, B., Liu, Z., Lu, S., & Yang, B. (2019). Biomass-derived carbon dots and their applications. *Energy & Environmental Materials*, *2*(3), 172-192. https://doi.org/10.1002/eem2.12038

Mies, M. J. M., Rebrov, E. V., Jansen, J. C., De Croon, M. H. J. M., & Schouten, J. C. (2007). Hydrothermal synthesis of a continuous zeolite Beta layer by optimization of time, temperature and heating rate of the precursor mixture. *Microporous and mesoporous materials*, *106*(1-3), 95-106. https://doi.org/10.1016/j.micromeso.2007.02.032

Mollazade, S. (2017). Optimal model of cultivation and water demand with environmental considerations in agricultural sector of Yasoouj plain. *International Academic Journal of Economics*, 4(1), 32–40.

Nandini, G. K. (2024). IOT Use in a farming area to manage water conveyance. *Archives for Technical Sciences/Arhiv za Tehnicke Nauke*, (31). https://doi.org/10.70102/afts.2024.1631.016.

Of, P., Acid, S., From, C., Husk, R., Of, I., Catalytic, I. T. S., & In, P. (2017). Preparation of Solid Acid Catalyst from Rice Husk and by Abel Aklilu A Thesis Submitted to The School of Chemical and Bio-Engineering Presented in Fulfilment of the Requirement for the Degree of Master of Science (Process Engineering) Addis Ababa Univer. October.

Ozyilmaz, A. T. (2023). Conducting Polymer Films on Zn Deposited Carbon Electrode. *Natural and Engineering Sciences*, *8*(2), 129-139. https://doi.org/10.28978/nesciences.1342013

Park, S. Y., Lee, H. U., Park, E. S., Lee, S. C., Lee, J. W., Jeong, S. W., ... & Lee, J. (2014). Photoluminescent green carbon nanodots from food-waste-derived sources: large-scale synthesis, properties, and biomedical applications. *ACS applied materials & interfaces*, *6*(5), 3365-3370.

Peng, D., Qiao, S., Luo, Y., Ma, H., Zhang, L., Hou, S., ... & Xu, H. (2020). Performance of microbial induced carbonate precipitation for immobilizing Cd in water and soil. *Journal of hazardous materials*, *400*, 123116. https://doi.org/10.1016/j.jhazmat.2020.123116

Prathumsuwan, T., Jaiyong, P., In, I., & Paoprasert, P. (2019). Label-free carbon dots from water hyacinth leaves as a highly fluorescent probe for selective and sensitive detection of borax. *Sensors and Actuators B: Chemical*, *299*, 126936. https://doi.org/10.1016/j.snb.2019.126936

Raghu, A. V., Karuppanan, K. K., & Pullithadathil, B. (2019). Highly surface active phosphorus-doped onion-like carbon nanostructures: ultrasensitive, fully reversible, and portable NH3 gas sensors. *ACS Applied Electronic Materials*, *1*(11), 2208-2219.

Rana, A., Alghazal, M. S., Alsaeedi, M. M., S. Bakdash, R., Basheer, C., & Al-Saadi, A. A. (2019). Preparation and characterization of biomass carbon–based solid acid catalysts for the esterification of marine algae

for biodiesel production. *BioEnergy Research, 12*, 433-442. https://doi.org/10.1007/s12155-019-9965-0

Reza, M. T., Andert, J., Wirth, B., Busch, D., Pielert, J., Lynam, J. G., & Mumme, J. (2014). Hydrothermal carbonization of biomass for energy and crop production. *Appl. Bioenergy*, *1*(1), 11-29.

Saha, B., & Abu-Omar, M. M. (2014). Advances in 5-hydroxymethylfurfural production from biomass in biphasic solvents. *Green Chemistry*, *16*(1), 24-38. https://doi.org/10.1039/C3GC41324A

Salame, P. H., Pawade, V. B., & Bhanvase, B. A. (2018). Characterization tools and techniques for nanomaterials. In *Nanomaterials for green energy* (pp. 83-111). Elsevier. https://doi.org/10.1016/B978-0-12-813731-4.00003-5

Shao, Y., Ding, Y., Dai, J., Long, Y., & Hu, Z. T. (2021). Synthesis of 5-hydroxymethylfurfural from dehydration of biomass-derived glucose and fructose using supported metal catalysts. *Green Synthesis and Catalysis*, *2*(2), 187-197. https://doi.org/10.1016/j.gresc.2021.01.006

Tiong, Y. W., Yap, C. L., Gan, S., & Yap, W. S. P. (2020). Kinetic and thermodynamic studies of oil palm mesocarp fiber cellulose conversion to levulinic acid and upgrading to ethyl levulinate via indium trichloride-ionic liquids. *Renewable Energy*, *146*, 932-943. https://doi.org/10.1016/j.renene.2019.07.024

Yi, G., Teong, S. P., Li, X., & Zhang, Y. (2014). Purification of biomass-derived 5-hydroxymethylfurfural and its catalytic conversion to 2, 5-furandicarboxylic acid. *ChemSusChem*, *7*(8), 2131-2135. https://doi.org/10.1002/cssc.201402105

Yu, H., Niu, S., Lu, C., Li, J., & Yang, Y. (2017). Sulfonated coal-based solid acid catalyst synthesis and esterification intensification under ultrasound irradiation. *Fuel*, *208*, 101-110. https://doi.org/10.1016/j.fuel.2017.06.122

Zhang, T., Fan, W., Li, W., Xu, Z., Xin, H., Su, M., ... & Ma, L. (2017). One-Pot Conversion of Carbohydrates into 5-(Hydroxymethyl) furfural using Heterogeneous Lewis-Acid and Brønsted-Acid Catalysts. *Energy Technology*, *5*(5), 747-755. https://doi.org/10.1002/ente.201600492

Zhang, Z., Zhen, J., Liu, B., Lv, K., & Deng, K. (2015). Selective aerobic oxidation of the biomass-derived precursor 5-hydroxymethylfurfural to 2, 5-furandicarboxylic acid under mild conditions over a magnetic palladium nanocatalyst. *Green Chemistry*, *17*(2), 1308-1317.

Zhu, C., Zhai, J., & Dong, S. (2012). Bifunctional fluorescent carbon nanodots: green synthesis via soy milk and application as metal-free electrocatalysts for oxygen reduction. *Chemical communications*, *48*(75), 9367-9369.

Zümrütdal, E., Zarifi, F., Yiğittekin, E. S., İstifli, E. S., Mertoğlu, T. Ş., Türüt, N., ... & Kılınççeker, G. (2022). Effect of Activated Carbon in Yogurt Production. *Natural and Engineering Sciences*, *7*(1), 1-21. https://doi.org/10.28978/nesciences.1098648